2001 India-USA Symposium on
Emerging Trends in Vibration and Noise Engineering

Structure-borne Noise Measures for a Multi-Dimensional Vibration Isolation System

Rajendra Singh and Seungbo Kim
Acoustics and Dynamics Laboratory
Department of Mechanical Engineering and
The Center for Automotive Research
The Ohio State University
Columbus, Ohio 43210-1107, USA

Abstract

This article examines alternate vibration isolation measures for a multi-dimensional system. The isolator and receiver are modeled by the continuous system theory. Source is assumed to be rigid and both force and moment excitations are considered. Our analysis is limited to a linear time-invariant system, and the mobility synthesis method is adopted to describe the overall system behavior. Inverted 'L' beam and plate receivers are employed here to incorporate the contribution of their in-plane motions to vibration powers and radiated sound. Multi-dimensional transmissibilities and effectivenesses are comparatively evaluated along with power-based measures for the inverted 'L' beam receiver and selected source configurations. Further, sound pressures radiated from the inverted 'L' beam receiver are calculated and correlated with power transmitted to the receiver. Interactions within the 'L' beam receiver are also analyzed and measures that could identify dominant transfer paths within a system are examined. Sound measurements and predictions for the inverted 'L' plate receiver demonstrate that a rank order based on free field sound pressures may be regarded as a measure of isolation performance. Measured insertion losses for sound pressure match well with those based on computed results. Finally, several emerging research topics are identified.

1. Introduction

Force or velocity transmissibility and related concepts are widely used, mostly for uni-directional motions [1-5] but have been extended to multi-dimensional systems [6]. Also, the force or velocity effectiveness term, the ratio of transmitted force or velocity with an isolator to the one without the isolator, has been employed for both uni-directional [1, 2, 4] and multi-dimensional problems [7, 8]. However, for a multi-dimensional problem, the units of translational and rotational quantities are not compatible [9-11]. For this reason, the concept of vibration power has been used to assess transmission to receivers [12, 11-16]. Application of such measures includes structural discontinuities [17-18], vibration isolators [11-16], and bearings [19]. The

transmission efficiency, the ratio of input vibration power to transmitted power, has been studied for propagating waves at the interface of infinite structures [17-18]. Input and transmitted powers have also been compared for some finite structures [15, 20-21].

For a multi-dimensional system, strong interactions occur between the coupled degrees-of-freedom. For example, Cremer and Heckle [17] claim that the moment mobility must be dealt with via a matrix in the presence of flexural motions. They have also explained that the coupling mobility in flexural motions may suppress the bending waves under some conditions. This concept has been implemented to attenuate vibration input to a single structure [9]. Further, some separation of transfer paths has been experimentally investigated [22]. Nonetheless, a proper quantification or interpretation of dynamic interactions that occur among coupled structural paths has not been addressed. Furthermore, the quantification of structure-borne energy and source strengths still remain as key obstacles in many cases [23-27]. Satisfactory resolution of such research issues would require appropriate vibration transmission measures. However, such measures for a multi-dimensional system are not well understood and often left to the discretion of user [1, 7, 28]. In this article, we address this particular issue with emphasis on a multi-dimensional isolator (of distributed parameters) in the presence of a compliant receiver.

2. Problem formulation

Problem is defined via Figures 1 and 2, in the context of source, path (isolator) and receiver. The scope of this study is limited to the analysis of a linear tme-invariant (LTI) system with a single isolator (defined in terms of distributed parameter). In this multi-dimensional system, the source is described by a rigid body and two alternate compliant receivers, namely the inverted ‘L’ beam and plate structures, are utilized for analytical and experimental studies. Harmonic force and moment excitations are applied to the source, up to 2.5 kHz. Mobilities of each component are analytically or computationally obtained, and then the mobility synthesis method is employed to predict the harmonic response of the overall system, based on the formulation reported in our earlier article [29]. Source characteristics that have been previously investigated are also utilized here [12]. Chief objectives of this study include: 1. Examine alternate measures of vibration isolation performance for a multi-dimensional system and quantify the vibration transmission for several system configurations. 2. Calculate and measure the sound generated from the ‘L’ structure receiver and correlate results with vibration isolation measures. Key concepts will be illustrated via experimental and analytical studies on selected isolators. All mathematical symbols are defined in Appendix A.

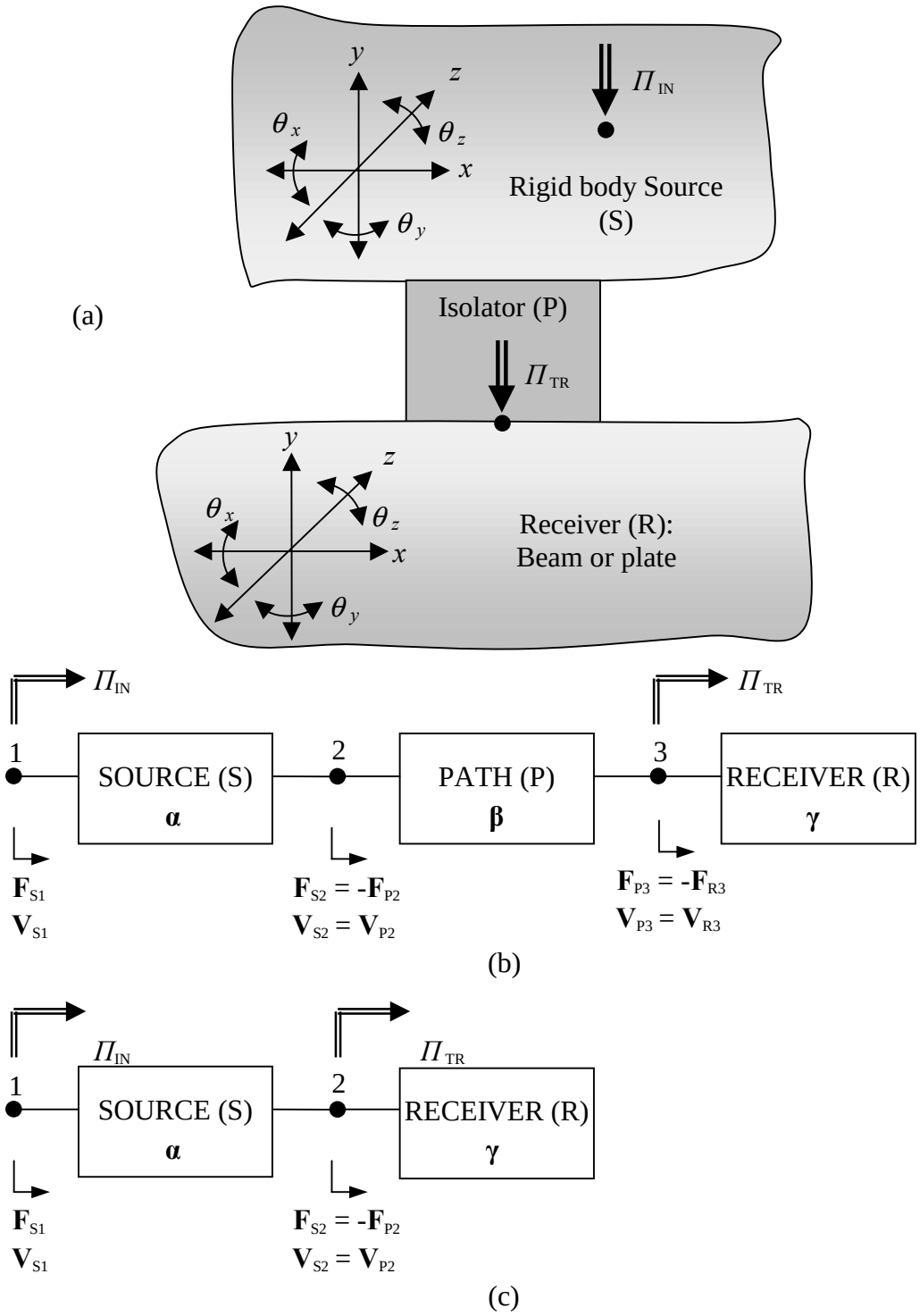

Figure 1. Problem formulation for vibration transmission. (a) Multi-dimensional path isolator; (b) source-path-receiver system and their mobility matrices **α, β** and **γ**; (c) vibration system without isolator. Here **F** and **V** are vectors.

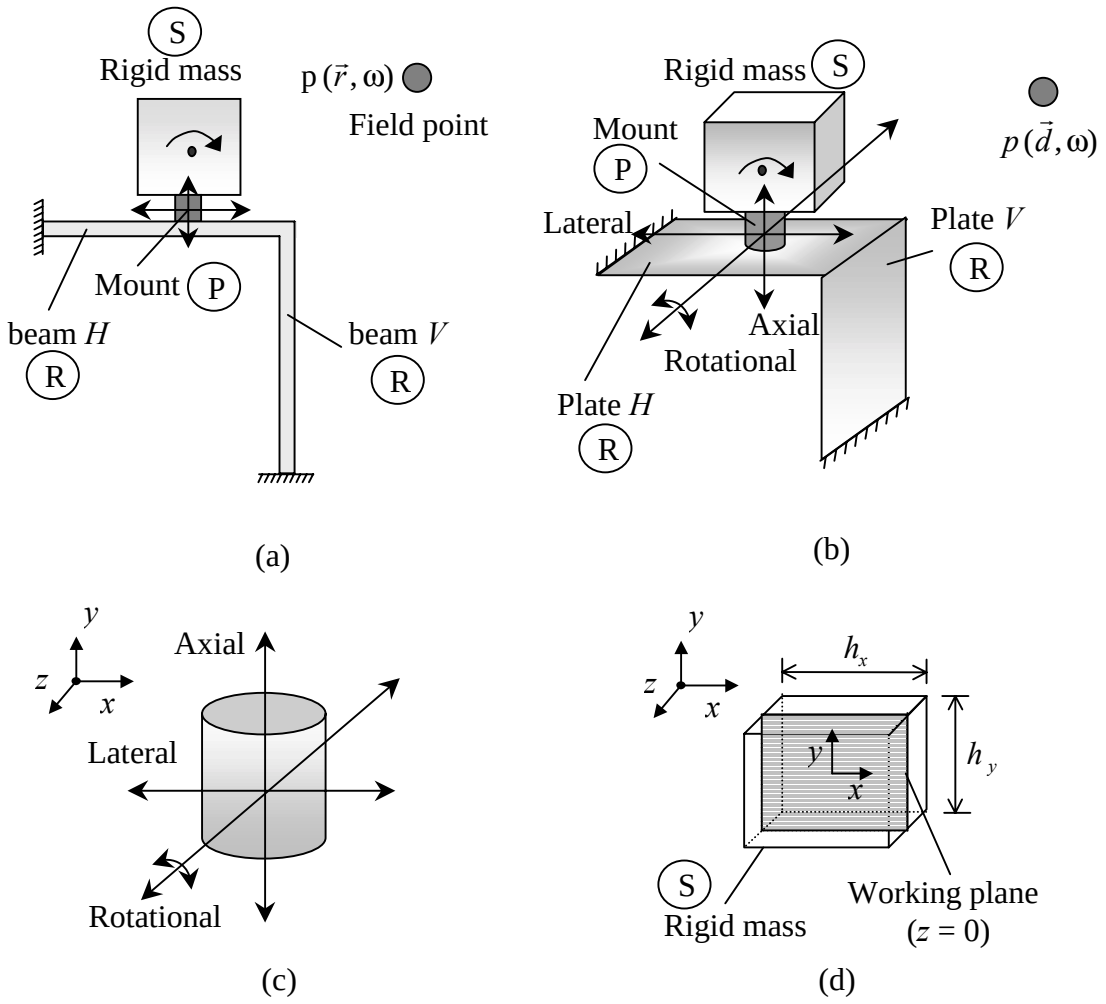

Figure 2. Configuration of the analytical vibration isolation system. (a) System with an inverted 'L' beam receiver; (b) System with an inverted 'L' plate receiver; (c) a cylindrical isolator with vibration transmission components; (d) isolator location [x , y , z] on the working plane of a cubic rigid body source: case 1 = [0, 0, 0]; case 2 = [0, $-h_y/2$, 0]; case 3 = [$-h_x/2$ $-h_y/2$, 0]; case 4 = [$-h_x/2$, 0, 0].

3. Vibration isolation measures for a multi-dimensional system

3.1 Vibration isolation measures

Vibration isolation measures are described in Table 1 for multi-dimensional motions; some explanations are also provided along with citation to literature. Detailed formulations are given in the recent manuscript we have submitted [30].

Measure	Definition as a function of ω
Force and motion transmissibilities [6, 8]	$\mathbf{TR}_F = \mathbf{F}_{\mathrm{R3}} / \mathbf{F}_{\mathrm{S1}}$ and $\mathbf{TR}_V = \mathbf{V}_{\mathrm{R3}} / \mathbf{V}_{\mathrm{S1}}$
Modified force and motion transmissibilities	$\mathbf{TR}_F^b = \mathbf{F}_{\mathrm{R3}} / \mathbf{F}_{\mathrm{P2}}^b$ and $\mathbf{TR}_V^f = \mathbf{V}_{\mathrm{R3}} / \mathbf{V}_{\mathrm{S2}}^f$
Force and motion Effectivenesses [7]	$\boldsymbol{\Xi}_{\mathbf{V}} = \lvert\mathbf{V}_{3,\mathrm{with}}\rvert / \lvert\mathbf{V}_{3,\mathrm{without}}\rvert$ and $\boldsymbol{\Xi}_{\mathbf{F}} = \lvert\mathbf{F}_{3,\mathrm{with}}\rvert / \lvert\mathbf{F}_{3,\mathrm{without}}\rvert$
Mean square force and velocities at receiver input	$\Psi_F^2 = < F_3^2(t) >_t = \frac{1}{2} Re[\tilde{F}_3 \tilde{F}_3^*] = \frac{\lvert F_3 \rvert^2}{2}$ and $\Psi_V^2 = < V_3^2(t) >_t = \frac{1}{2} Re[\tilde{V}_3 \tilde{V}_3^*] = \frac{\lvert V_3 \rvert^2}{2}$
Weighted mean square force and velocities at receiver input	$\Psi_{WF,\mathrm{Total}}^2 = \frac{1}{2} Re[\tilde{\mathbf{F}}_3^{\mathrm{T}}\ diag[\mathbf{M}_{33}]\tilde{\mathbf{F}}_3^*]$ and $\Psi_{WV,\mathrm{Total}}^2 = \frac{1}{2} Re[\tilde{\mathbf{V}}_3^{\mathrm{T}}\ diag[\mathbf{Z}_{33}]\tilde{\mathbf{V}}_3^*]$
Power transmitted to receiver input [9-16, 19-21]	$\Pi_{\mathrm{TR}}(\omega) = \frac{1}{2} Re[\mathbf{F}^{\mathrm{T}}\mathbf{V}^*] = \frac{1}{2} Re[\mathbf{V}^{\mathrm{T}}\mathbf{F}^*]$
Efficiency of vibration power transmitted to receiver input [15, 20, 21]	$\Gamma(\omega) = \frac{\Pi_{\mathrm{TR}}}{\Pi_{\mathrm{IN}}}$
Effectiveness of vibration power transmitted to receiver input [21, 20]	$\Xi_{\Pi}(\omega) = \frac{\Pi_{\mathrm{TR,\ with}}}{\Pi_{\mathrm{TR,\ without}}}$
Vibration or sound amplitudes at the receiver	$F(\omega)$, $V(\omega)$ or $p(\omega)$
Insertion loss [1, 2]	$IL_{Q_i} = 10\log_{10}(\frac{\Psi_{Q_i,A}^2}{\Psi_{Q_i,B}^2})$, dB

Table 1. Summary of frequency domain vibration isolation measures for multi-dimensional motions. See notes below for some explanations.

Notes.

1. Subscripts 1, 2, 3 and 4 are input, interfacial and output locations of components as shown in Figure 1.
2. Operator '/ ' is a quotient operation for vectors.
3. Superscripts *b* and *f* represent blocked and free boundary conditions at the source output respectively.
4. Operators $<>_t$ and *diag* represent time averaged quantity and diagonal matrix of the original matrix respectively.
5. Subscripts 'with' and 'without' represent a system with an isolator and without any isolator respectively. Refer to Figures 1(b) and 1(c).
6. Subscripts IN and TR represent input at source and transmitted power at receiver input respectively.
7. $Q_i = p_i(\omega), F_i(\omega)$ or $V_i(\omega)$ at *i*. Also, A and B represent two different physical systems.

3.2 System with an inverted 'L' beam receiver

3.2.1 System configuration

Various vibration isolation measures are examined for an analytical isolation system with an inverted 'L' beam receiver of Figure 2(a). Note that longitudinal motion of one beam is coupled with flexural motion of the other and thus both contribute to sound radiation. The four isolator attachment cases of Figure 2(d) are analyzed up to 3 kHz. These cases provide several transmission configurations even though cases 3 and 4 are statically unstable and case 1 is physically meaningful only for three-dimensional motions in terms of its implementation. Nonetheless, vibration transmitted to receiver is strongly affected by the mount location, and thus by the free velocity of source [12].

The isolator is connected to the inverted 'L' beam at $0.75\ell_H$ where ℓ_H is the length of the horizontal beam. This off-center location highlights the effect of coupling mobility of receiver. Note that such a coupling mobility term does not exist for a centrally driven beam (with symmetric boundaries) and for an infinite beam. The isolator of Figure 2(c) is modeled using the Timoshenko beam theory to describe flexure along with the wave equation for longitudinal motion. Thus, the effects of shear deformation and rotary inertia are included. Mobilities of the Timoshenko beam have been analyzed for two types of solution in an earlier paper by the same authors [21]; the resulting formulations are used here. Material properties such as shear modulus (*G)*, the mass density (ρ) and Poisson's ratio (ν) of the isolator are listed in Table 2.

Property or dimension	Source (Cubic rigid body)	Isolator (Circular beam)	Inverted 'L' beam Receiver
m (kg)	1	-	-
E (MPa)	-	16.2	6.688×10^4
G (MPa)	-	5	-
η	-	0.3	0.001
ρ (kg/m^3)	-	1,000	2,723
Dimensions in mm	ℓ = 50	ℓ = 30 r = 12	ℓ = 400, b = 100, t = 5 (horizontal and vertical beam)

Table 2. Material properties and dimensions of the analytical system of Figure 2(a).

The modulus of elasticity E for the rubber material is found from the relation $E = 3G(1+QT^2)$ where Q is a numerical constant and T is the isolator shape factor [3]. For a circular rubber cylinder, Q is 2 and T is equal to $2r/(4\ell)$ where radius (r) and length (ℓ) values are listed in Table 2 [3]. Also, a frequency-invariant loss factor η of 0.1 is assumed to incorporate damping within the isolator. It is included in the calculation with the complex-valued modulus of elasticity as $\tilde{E} = E(1+j\eta)$. Also, a loss factor of 0.002 is used to represent a lightly damped structure and included in $\tilde{E}$. Harmonic responses of the inverted 'L' beam are obtained by synthesizing the mobilities of each beam, with reference to Figure 3(a). Details are given in reference [30].

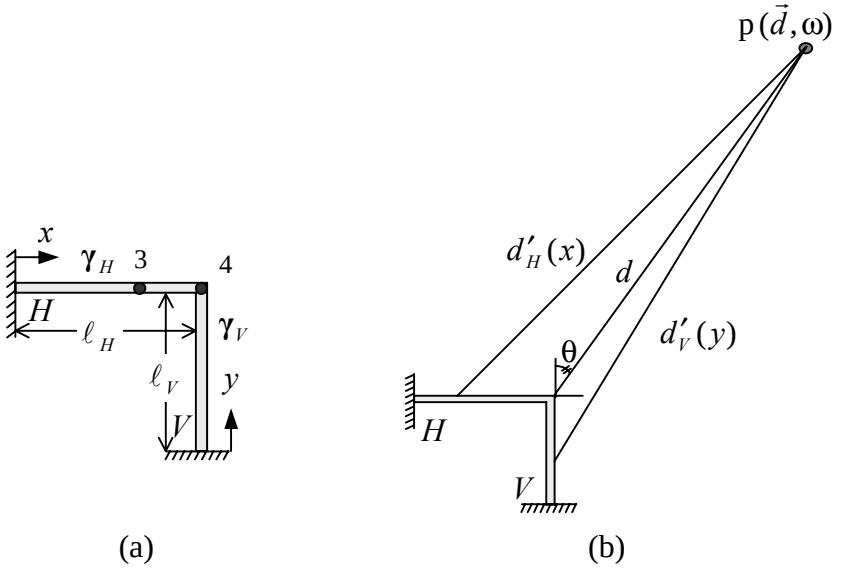

Figure 3. Sound radiation from an inverted 'L' beam receiver. (a) 'L' beam configuration and its mobilities; (b) acoustic field point. Here, location 3 is interface of receiver with an isolator, and interface between beams H and V is denoted by location 4.

3.2.2 Vibration isolation measures using TR or Ξ

Force and velocity transmissibilities (TR) are computed using the inverted 'L' beam receiver, with only one isolation configuration (case 2) of Figure 2(d). Only non-dimensional diagonal terms in transmissibility matrices are analyzed. First, TR_F and TR_F^b spectra are shown in Figure 4 and both force transmissibilities show similar patterns.

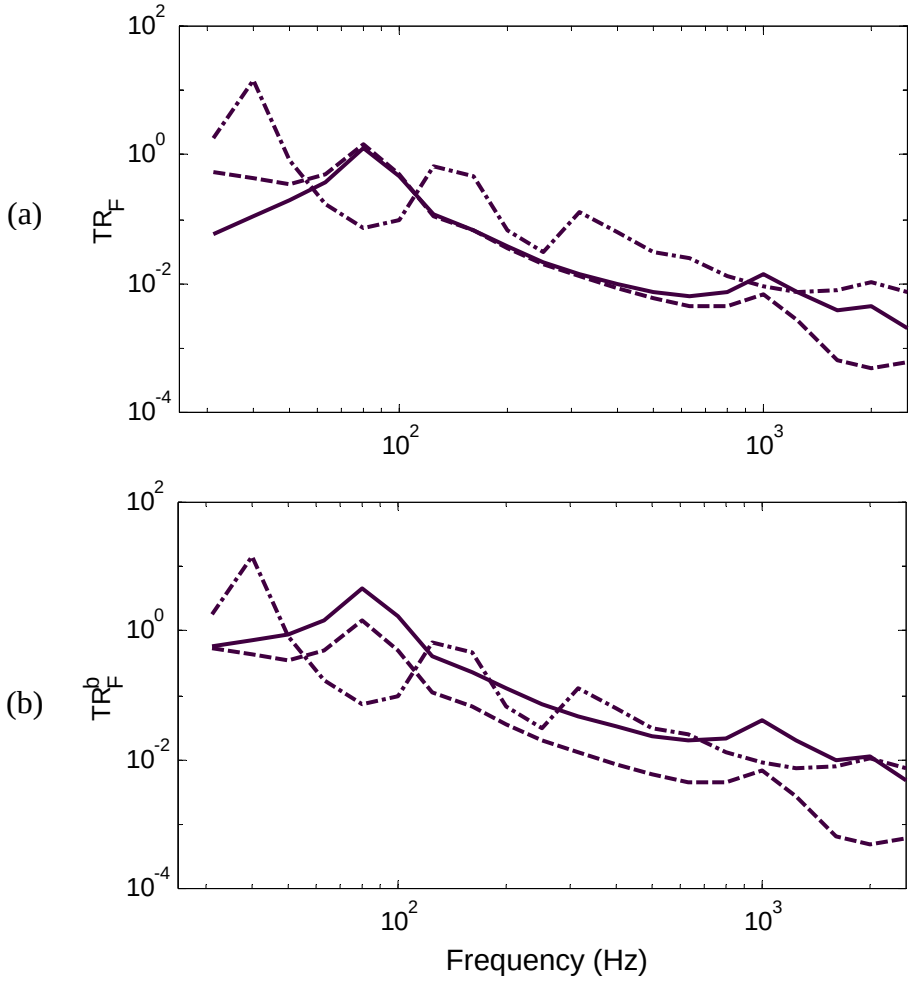

Figure 4. Force transmissibility with an inverted 'L' beam receiver and case 2 isolator. (a) Force transmissibility TR_F; (b) modified force transmissibility TR_F^b. Key: ———, f_x; –·–·–·–, f_y; --------, q_z.

Next, the velocity TR_V and modified velocity TR_V^f transmissibilties are shown in Figure 5. The differences between the TR_V and TR_V^f components are more pronounced than the ones between TR_F and TR_F^b. This is because the axial components of TR_V and TR_V^f dominate over the entire frequency range and the lateral components of TR_V and TR_V^f are higher than the rotational component of those. Also, the difference between lateral and rotational components is reduced in the TR_V^f calculations.

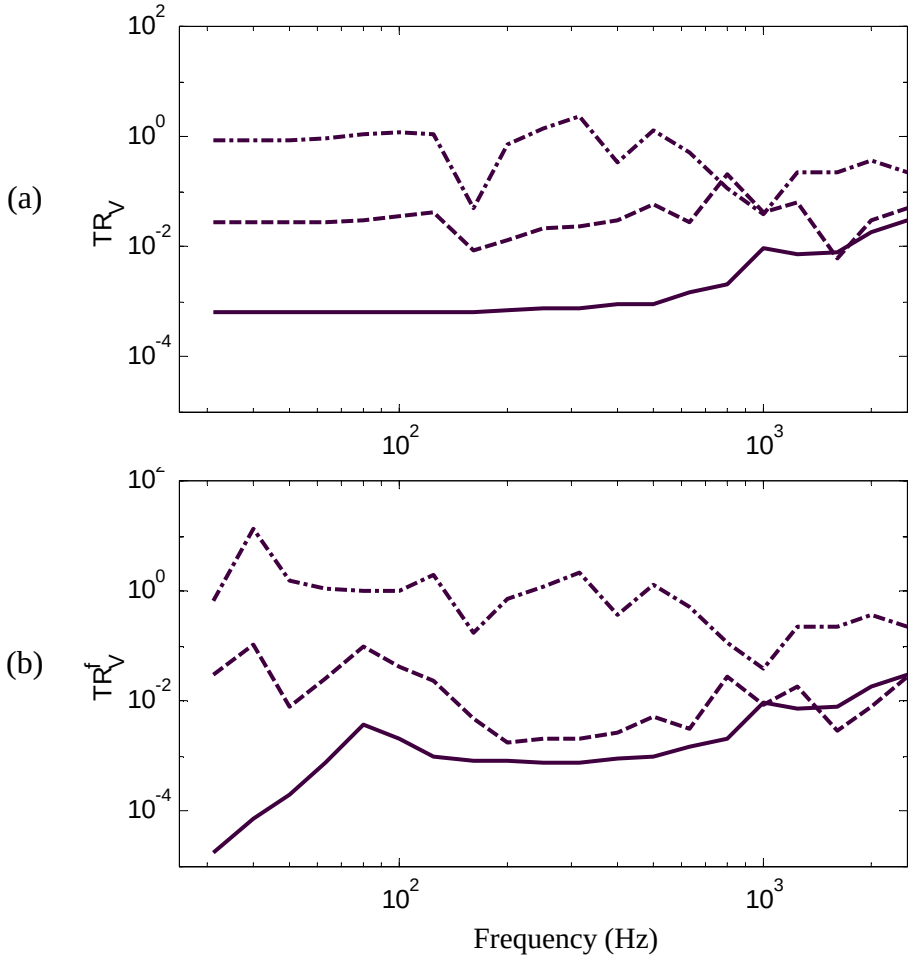

Figure 5. Velocity transmissibility with an inverted 'L' beam receiver and case 2 isolator. (a) Velocity transmissibility TR_V; (b) modified Velocity transmissibility TR_V^f. Key: ———, f_x; –·–·–·, f_y; --------, q_z.

Finally, the Ξ_F and Ξ_V effectiveness spectra are shown in Figure 6. The rank ordering of components based on Ξ_F and Ξ_V is similar to the one observed with force and velocity transmissibilties. However, it is observed that the rotational component increases and is higher than the lateral component in Ξ_F and Ξ_V spectra as ω increases.

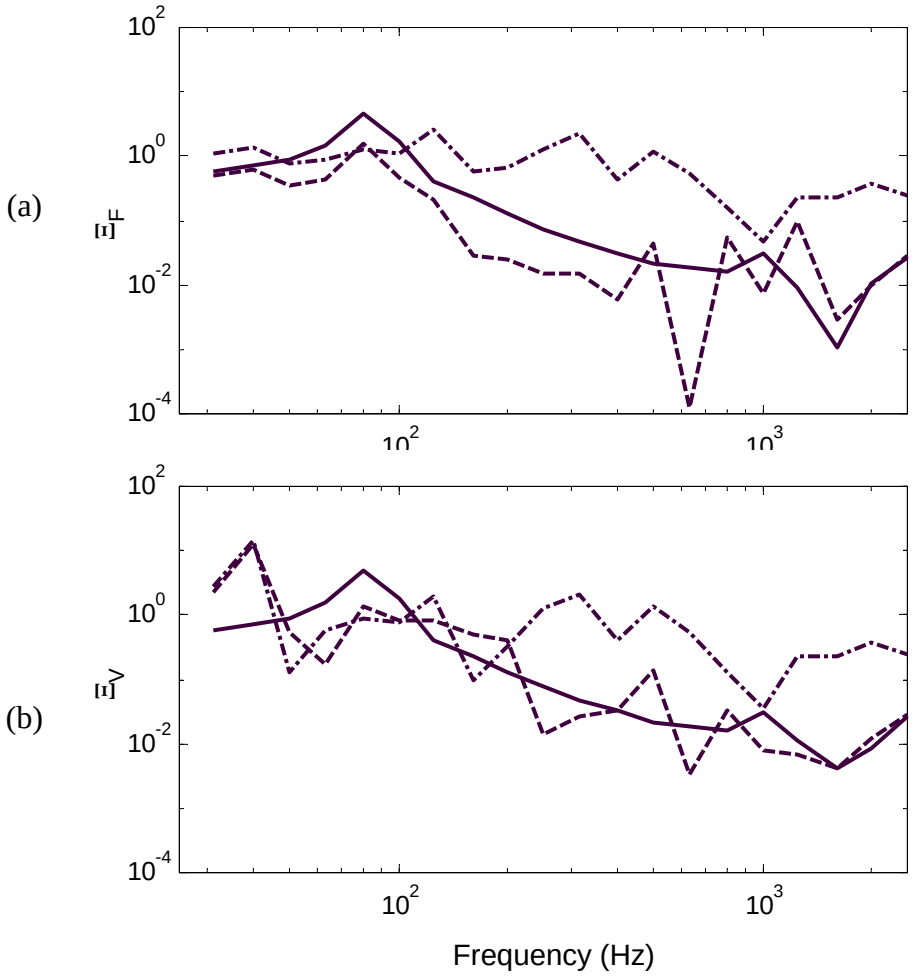

Figure 6. Force and velocity effectiveness with an inverted 'L' beam receiver and case 2 isolator. (a) Force effectiveness Ξ_F; (b) velocity effectiveness Ξ_V. Key: ———, f_x; –·–·–··, f_y; --------, q_z.

3.2.3 Power-based vibration isolation measures

The four different cases of the isolator connection, as shown in Figures 2(d), are investigated using the same component parameters. Vibration power transmitted to receiver are computed and analyzed up to 3 kHz. Total vibration powers Π_{Total} transmitted to the 'L' beam receiver are compared in Figure 11(a) for the 4 location cases of Figure 2(d). It is observed that total vibration powers for cases 3 and 4 are almost the same but these are higher than those for cases 1 and 2. Also, the transmitted power is lowest among the cases considered when the isolator is attached to mass center of rigid body (case 1).

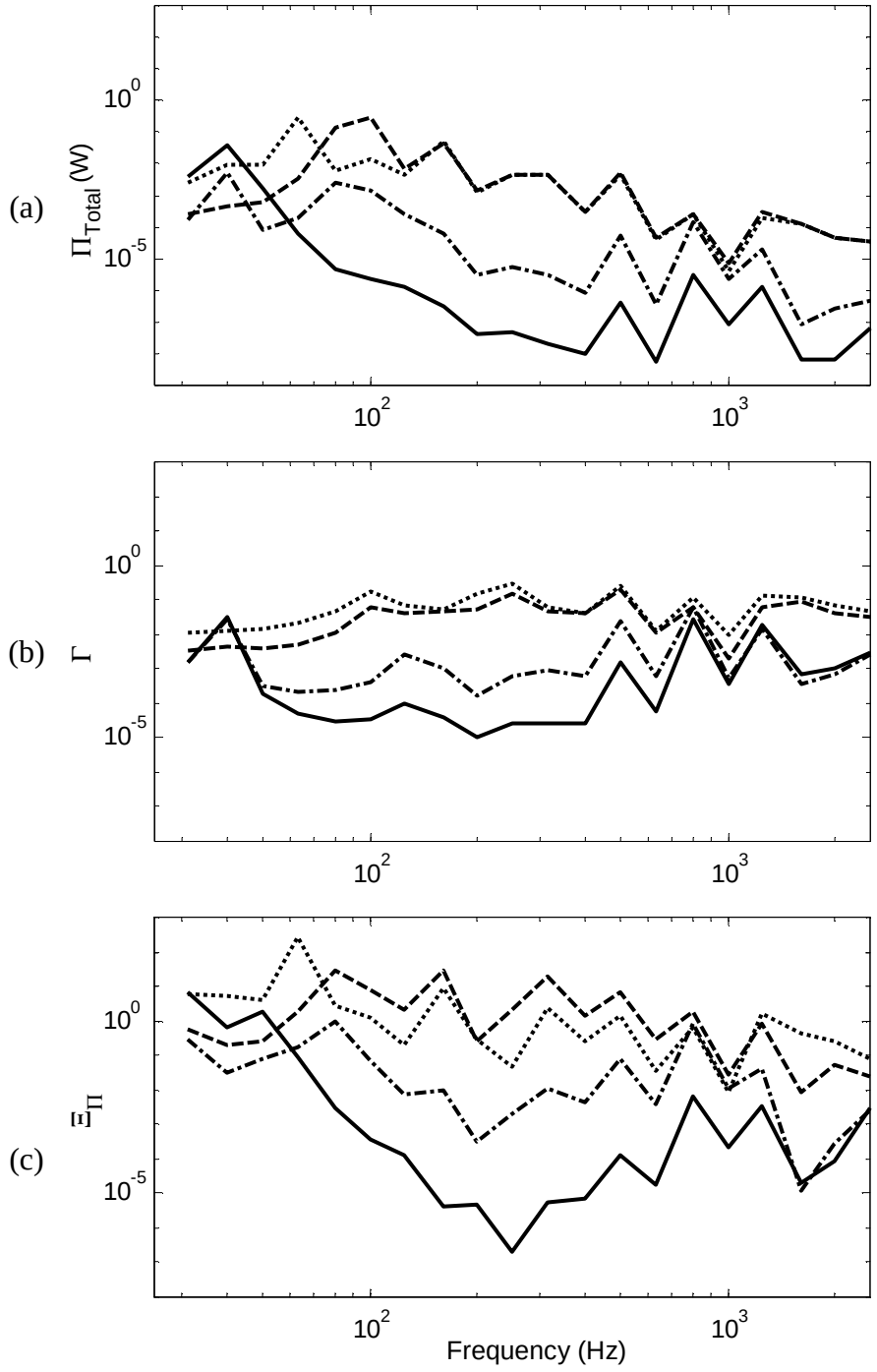

Figure 11. Vibration isolation measures with an inverted 'L' beam receiver given moment excitation. (a) Total transmitted vibration power Π_{Total}; (b) efficiency Γ for total transmitted vibration power; (c) effectiveness Ξ_Π for total transmitted vibration power. Key: ——— , mount location case 1; –·–·–·–, case 2; - - - - - - - -, case 3; ····· , case 4.

The power efficiencies Γ are shown in Figures 11(b), and a rank order based on Γ is similar to the one given by Π_{Total}. However, Γ in case 1 rises and is higher than the one for case 2 as ω increases. Also, for all cases, overall characteristics of Γ rise as ω increases even though the value of Π_{Total} decreases. The power effectivenesses Ξ_{Π} are also shown in Figure 11(c). The patterns for Ξ_{Π} spectra do not exactly match with Π_{Total} for the cases considered. For example, The Ξ_{Π} for case 3 is higher than the one of case 4 at low frequencies but is lower at high ω.

3.2.4 Sound radiation from receiver as a measure of vibration isolation

Sound pressure p at a selected point in free field ($\vec{d}$) is calculated in order to examine its relationship with vibration power transmitted to the receiver of Figure 2(a). An inverted 'L' beam is chosen as the chief radiating structure and it will incorporate contributions from longitudinal and flexural structural powers.

Calculated mean-square sound pressures (Ψ_p^2) are shown in Figure 12 for four cases. Horizontal beam is connected to the isolator at $3\ell_H/4$ from its clamped end. The field point is located at d = 1 m from the intersection of two beams, at 45^o from the outer surfaces of each beam, as shown in Figure 3(b). The rank order associated with four locations and related sound pressure spectral shapes match the transmitted vibration power spectra of Figure 11(a).

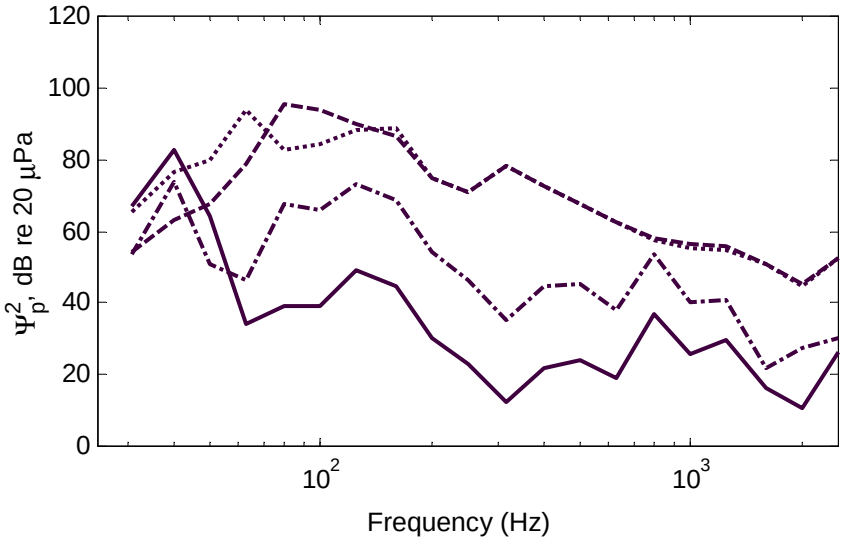

Figure 12. Far field sound pressures radiated by the 'L' beam of Figure 16. Key:———, mount location case 1;–·–·–·–·-, case 2;- - - - - - - -, case 3; ····· , case 4.

4. Experimental system with an Inverted ‘L’ plate receiver

4.1 System configuration

Similar to the inverted ‘L’ beam receiver, an inverted ‘L’ plate receiver, as shown in Figure 13, is employed to describe both in-plane and out-of plane motion transmissions to the receiver. Overall, 4 isolators of Figure 13(c-d) are experimentally studied. The material properties and dimensions of the source, isolator and receiver are summarized in Table 3. Each isolator is located at either the center or edge of mass to realize different vibration isolation configurations. However, the mount location on the receiver side is unchanged. The field point ($\xi_1 = \vec{d}$) for sound pressure measurements $p(\omega)$ is located at a distance of 0.2 m from the mating edge of two plates, at 45º from the outer surfaces. Sound pressures at other field locations (ξ) and structural velocities at selected points (ξ) on the receiver plates are also examined, as summarized in Table 4. Figure 14 shows the modified experimental schematic used for moment driven responses where a phase shifter is used. Table 5 lists the instruments used. Measurement are conducted in an anechoic room under the sine sweep excitation (up to 3 kHz). In-phase and 180º out-of-phase forces (in *y* direction) are separately applied to the edges of the rigid source to simulate the force (f_y) and moment (q_z) excitations at *G* respectively. Forces from two shakers and accelerations at the driving point locations are measured using two impedance heads. Plastic and steel stingers are used over low (up to 1 kHz) and high (1 – 3 kHz) frequency regimes respectively since the dynamic forces could not excite the system above 1 kHz with plastic stingers. Typical force signals are shown in Figure 15. The input forces with almost the same magnitudes and 180º (or 0º) phase difference are maintained throughout the experiments for moment (or force) excitation cases as shown in Figure 16. However, the phase between two forces deviates slightly from 180º (or 0º) at a system resonance (approximately 600 Hz). This resonance appears to be a result of the experimental system dynamics with two shakers. Forces measured at the driving point locations are used for computational predictions.

The mobilities of the inverted ‘L’ plate structure are obtained by using a commercial finite element (FEA) IDEAS [31] code. Further, interfacial forces and moments between the isolator and receiver are calculated by synthesizing the mobilities of the inverted ‘L’ plate, source and isolator. Then, the plate velocity distribution from FEA calculation is provided to a commercial boundary element method (BEM) SYSNOISE [32] code to predict the sound radiation. Individual sound fields generated by each plate for interfacial forces and moments are superimposed to determine the resultant sound pressure. Note that direct radiation from either source or isolator is not included in such calculations. Overall, sound pressure and velocity amplitudes at locations of Table 4 are obtained using the FEA and BEM methods. Vibration power (Π_{TR}) transmitted to the ‘L’ plate and the power (Π_{RAD}) radiated to the acoustic medium from the receiver, as defined below, are also predicted:

$$\Pi_{\mathrm{RAD}} = \frac{1}{2} \int_A p\, v_a^*\, dS\,. \tag{1}$$

Here, p and v_a are sound pressure and the particle velocity amplitudes respectively at a control surface *S* [17, 33].

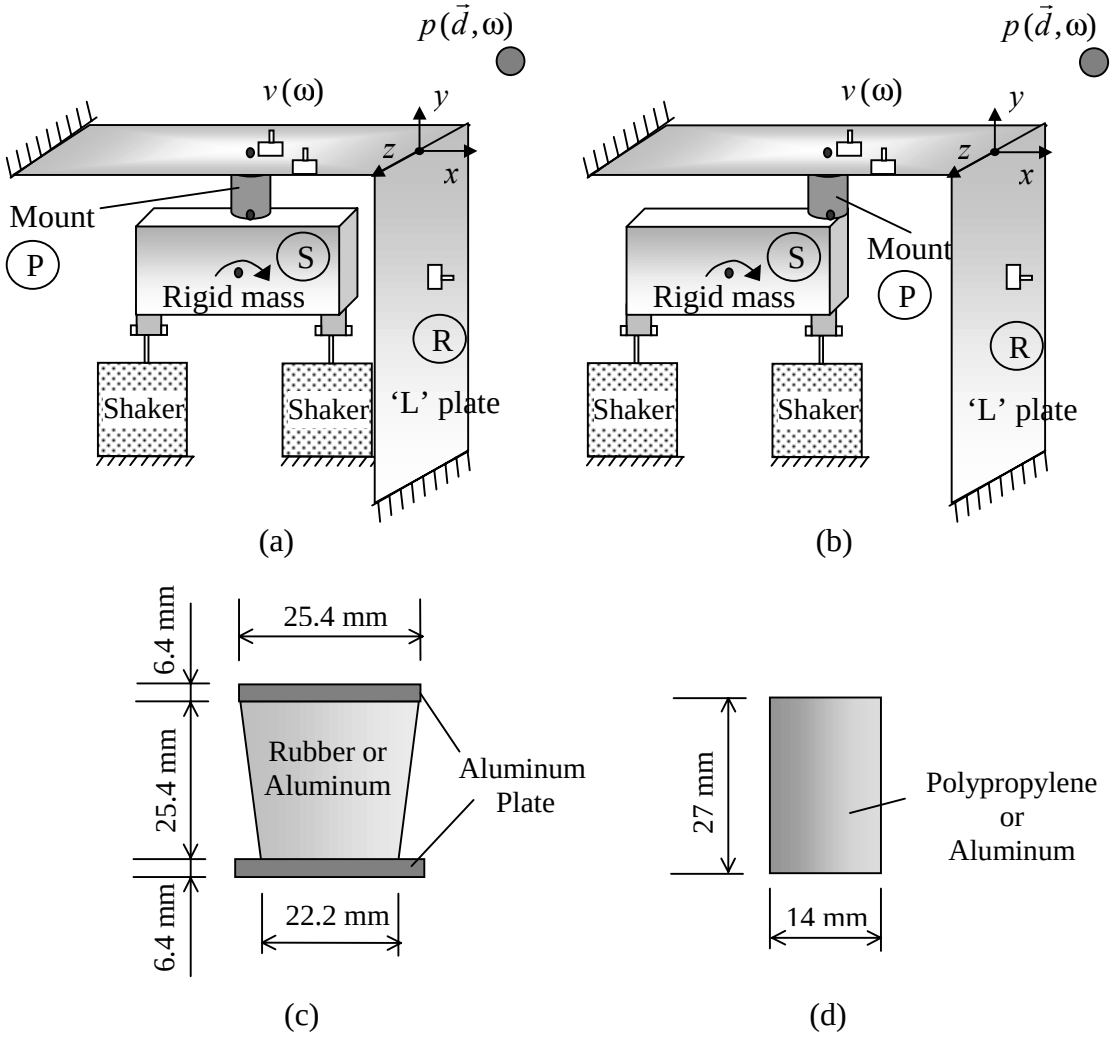

Figure 13. Experimental system with an inverted 'L' plate receiver, as excited by harmonic forces and moment. (a) System with rotational free velocity only; (b) system with translational and rotational free velocities; (c) Isolator I; (d) Isolator II.

Property or dimension	m *(kg)*	E *(MPa)*	*G* (MPa)	η	ρ (kg/m^3)	Dimensions in mm
Source (Rectangular rigid body)	1.2	-	-	-	-	ℓ = [*x*, *y*, *z*] = [140, 64, 47]
Rubber isolator I	-	2.8	0.8	0.2	1000	$\ell_{effective}$ = 35 $r_{effective}$ = 12
Aluminum isolator I	-	6.688×10^4	2.4×10^4	0.001	2723	$\ell_{effective}$ = 35 $r_{effective}$ = 12
Polypropylene isolator II	-	5	1.6	0.2	1000	ℓ = 27 *r* = 7
Aluminum isolator II	-	6.688×10^4	2.4×10^4	0.001	2723	ℓ = 27 *r* = 7
Inverted 'L' plate receiver	-	19.5×10^4	8.3×10^4	0.001	7700	ℓ = 400 *t* = 1 (Square horizontal and vertical plates)

Table 3. Material properties and dimensions of the experimental system of Figure 13. Note that rubber and polypropylene properties are approximate.

Location No.	Measure	Coordinates (m)	'L' structure location
ξ_1	Sound pressure	*x* = 0.14, *y* = 0.14, *z* = 0	Acoustic free field
ξ_2	Sound pressure	*x* = -0.18, *y* = 0.46, *z* = 0	Acoustic free field
ξ_3	Velocity	*x* = -0.15, *y* = 0, *z* = 0	Horizontal plate
ξ_4	Velocity	*x* = 0, *y* = -0.15, *z* = 0	Vertical plate

Table 4. Locations of vibration transmission measures

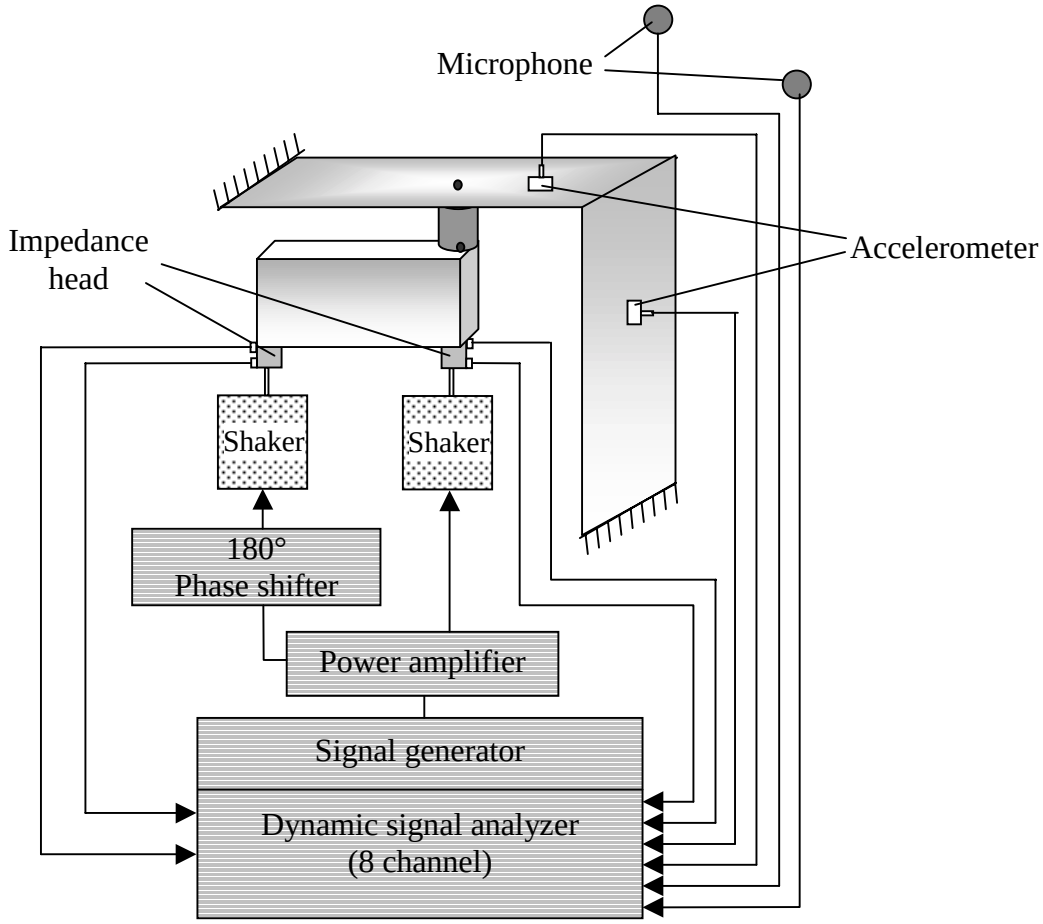

Figure 14. Experimental schematic for the source characteristics study of a system with an inverted 'L' plate receiver and sound radiated from receiver plate.

Item	Manufacturer	Model No.
Accelerometers	PCB	A353B66
Microphones	PCB	L130C10
Impedance heads	PCB	288D01
Shakers	Labworks	ET-132-2
Phase shifter	AVC Instrumentation	780M01
Power amplifiers	Electro-Voice	7300A
Dynamic signal analyzer (8 channel) with signal generator	HP	HP3566A

Table 5. List of instruments used for experimental studies

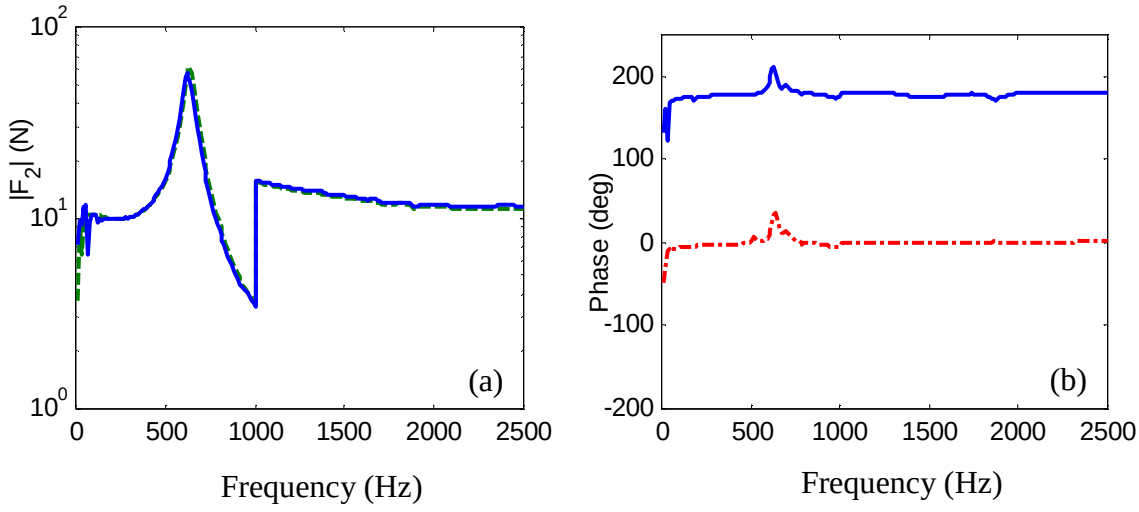

Figure 15. Typical force input to the mass source. (a) Force magnitude. Key: ——— , mount located at the edge of source; –·–·–·– , mount located at the center of source. (b) relative phase between two force inputs. Key: ——— , moment excitation; –·–·–·– , force excitation.

4.2 Effect of isolator materials

The effect of isolator material properties is quantified in terms of insertion losses (*IL*) for sound pressure (*p*), vibration velocity (*v*) and acoustic power (Π_{RAD}) are calculated where

$$IL_{p_i} = 10\log_{10}\left(\frac{\Psi^2_{p_i,A}}{\Psi^2_{p_i,B}}\right), \text{dB}; \qquad IL_{v_j} = 10\log_{10}\left(\frac{\Psi^2_{v_j,A}}{\Psi^2_{v_j,B}}\right), \text{dB}; \tag{2a-b}$$

$$IL_{\Pi_{RAD}} = 10\log_{10}\left(\frac{\Pi_{RAD,A}}{\Pi_{RAD,B}}\right), \text{dB}. \tag{2c}$$

Here, p_i and v_j are sound pressure at acoustic field point *i* and velocity at receiver structure location *j* respectively. Further, '*A*' and '*B*' represent the system with an aluminum and rubber (or polypropylene) isolator respectively. The IL_p and IL_v spectra are obtained from both experimental and computational studies but only the computed results are used for $IL_{\Pi_{RAD}}$. The results are given at the center frequencies of the 1/3 octave band. Each isolator of Figure 13(c-d) is separately examined and the mount location is unchanged for all cases. Experimental and computational results at the response locations (ξ) of Table 4 are shown in Figures 16 to 17 for isolators I and II respectively when force (*y*) is applied at the mass center of a rigid body source. Further, the measured force inputs are used for computational studies. Resulting vibration and acoustic measures can not be normalized with respect to their excitation forces since two different input forces are used. However, it is observed that measured input forces from the shaker stingers to a mass source do not vary much given different system configurations. Figures

16 and 17 show that vibration and noise transmissions are much reduced over a wide range of frequencies when a rubber isolator with a lower G is used in place of an aluminum isolator. Further, $IL_{\Pi_{RAD}}$ spectra for sound power radiated from the 'L' plate receiver match well with the IL_p spectra for sound pressure, especially at location ξ_1. However, the experiment results of IL_p do not exhibit as much reduction as the ones computed beyond 500 Hz. This is because the actual sound radiated from the receiver is lower than shaker noise beyond 500 Hz, especially when a rubber isolator is located at the center of source. See Figures 16(b) and 17(b) where the background noise from shakers is also shown with mean-square sound pressure (Ψ_p^2). Note that measured Ψ_p^2 of the system shows almost the same level as Ψ_p^2 of shakers as shown in Figures 16(b) and 17(b). Further, note that IL_v spectra, that are not contaminated by shaker noise, are much higher than IL_p beyond 500 Hz as shown in Figures 16(c-d) and 17(c-d). Observe that the IL_v from experiments reasonably match with predicted IL_v as shown in Figures 16(d-e) and 17(d-e). Figures 16 and 17 show that insertion losses at lower frequencies are higher than the ones at higher frequencies, unlike the analytical prediction reported in a recent article [21]. This is because the force inputs from shakers are not uniformly distributed over the frequency range and higher forces are supplied to the experimental system at lower frequencies than at higher frequencies as shown in Figure 15. Further note that we have assumed spectrally-invariant properties for the four isolator examples. Spectral averages of measured and computed results are shown in Table 6 for insertion losses. Overall, reasonable agreements between computed and experimental results are observed even though some measurements are contaminated by the shaker noise.

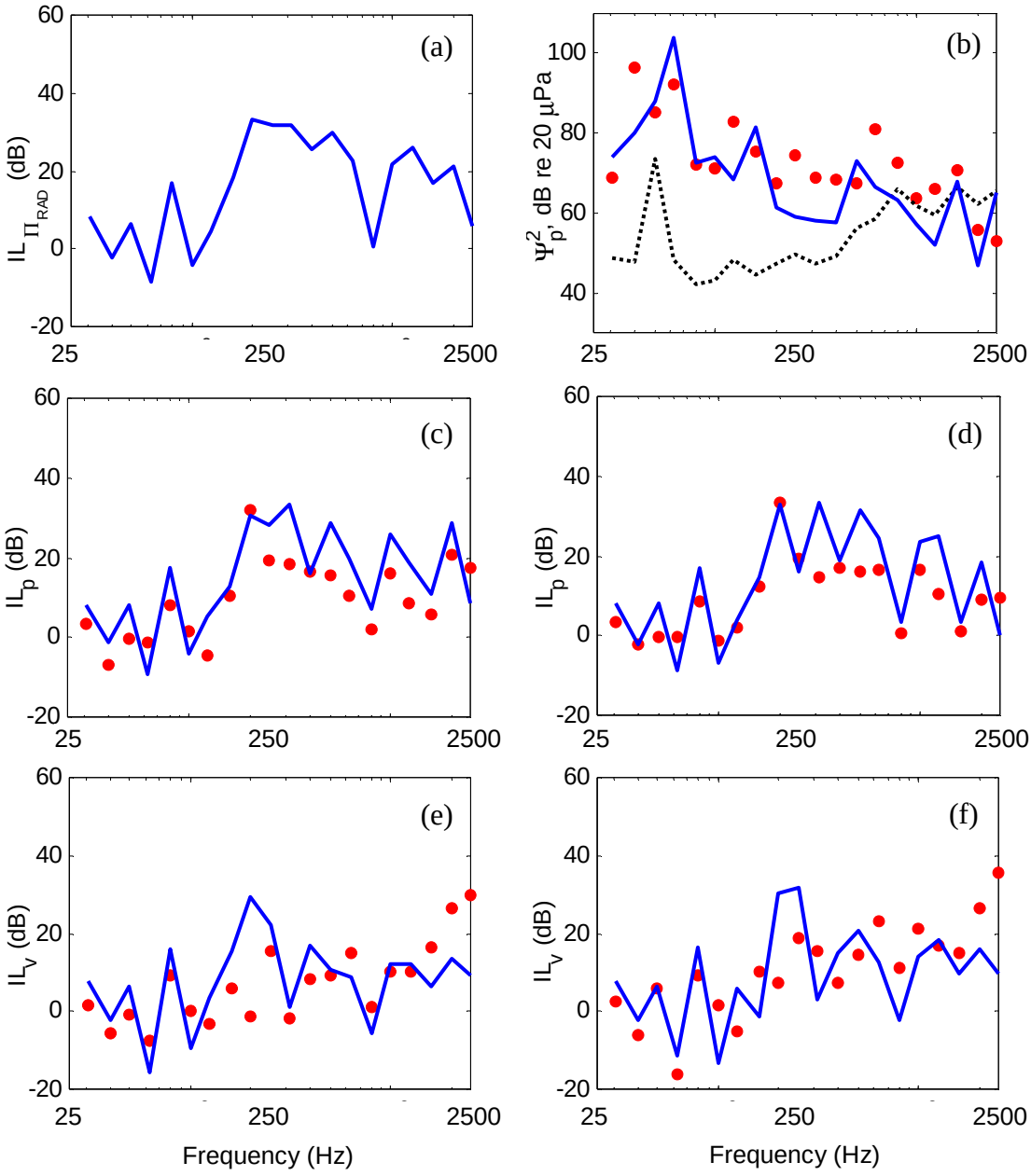

Figure 16. Vibration isolation measures on mount material effect for isolator I given force excitation. (a) Insertion loss ($IL_{\Pi_{RAD}}$) of acoustic power radiated from the 'L' plate receiver; (b) mean-square sound pressure (Ψ_p^2) at location ξ_1 of Table 4 with mount configuration of Figure 12(a); (c) insertion loss (IL_p) of sound pressure at field location ξ_1; (d) IL_p at location ξ_2; (e) insertion loss (IL_v) of velocity at plate location ξ_3; (f) IL_v at location ξ_4. Key: ———, calculated; ● , measured; ·····, background noise from shakers. Results are given in terms of 1/3 octave band center frequencies from 31.5 to 2500 Hz. Only the mean values within each bandwidth are plotted here.

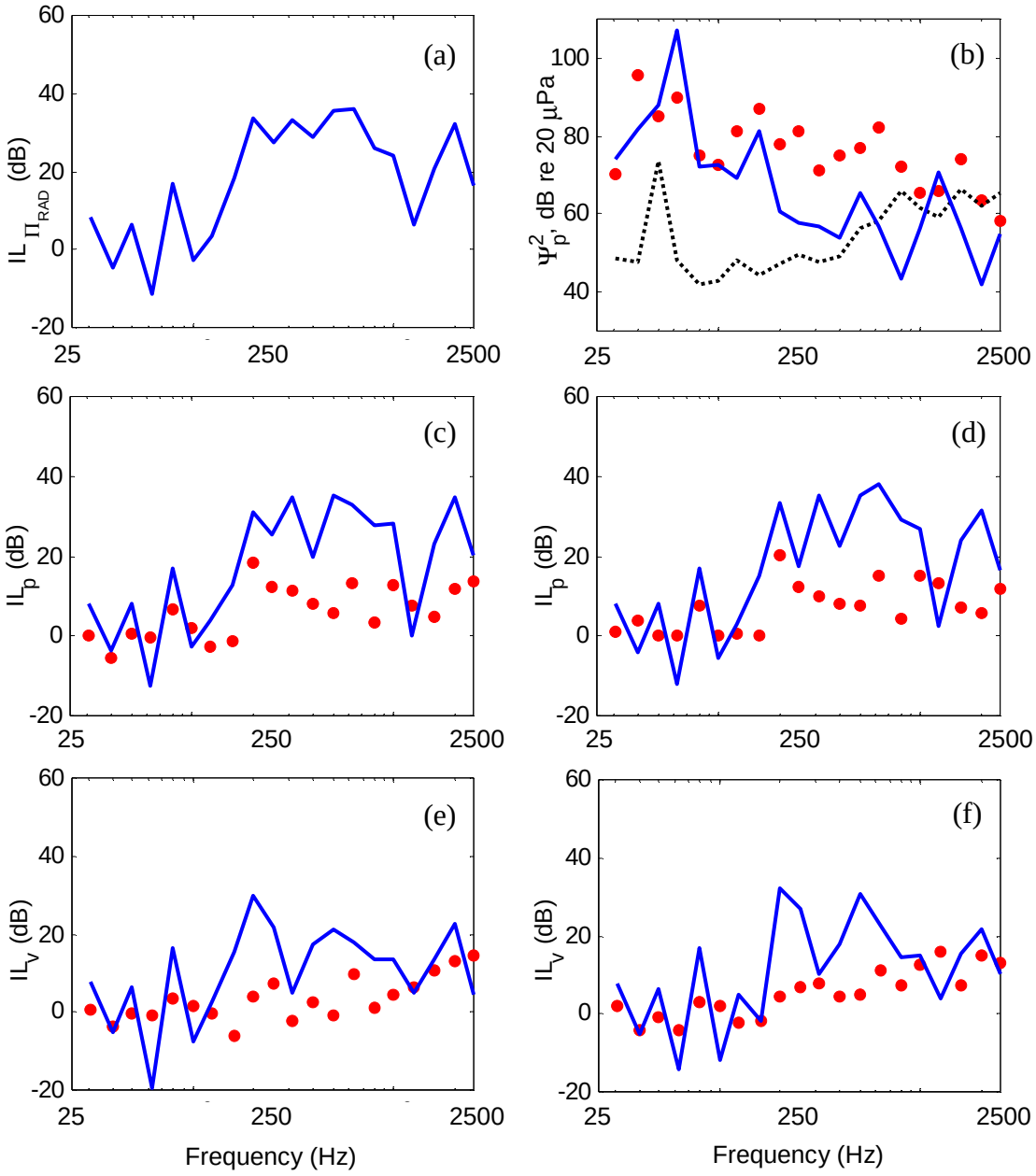

Figure 17. Vibration isolation measures on mount material effect for isolator II given force excitation. (a) Insertion loss ($IL_{\Pi_{RAD}}$) of acoustic power radiated from the 'L' plate receiver; (b) mean-square sound pressure (Ψ_p^2) at location ξ_1 of Table 4 with mount configuration of Figure 12(a); (c) insertion loss (IL_p) of sound pressure at field location ξ_1; (d) IL_p at location ξ_2; (e) insertion loss (IL_v) of velocity at plate location ξ_3; (f) IL_v at location ξ_4. Key: ——— , calculated; ● , measured; ..... , background noise from shakers. Results are given in terms of 1/3 octave band center frequencies from 31.5 to 2500 Hz. Only the mean values within each bandwidth are plotted here.

Effect	Measure (Mean-square value)	Isolator	Computation (dB)		Experiment (dB)	
			at ξ_1 or ξ_3	at ξ_2 or ξ_4	at ξ_1 or ξ_3	at ξ_2 or ξ_4
Isolator material given force excitation	Velocity (Ψ_v^2) at ξ_3 or ξ_4	Isolator I *	8	9	7	11
		Isolator II **	10	11	3	5
	Sound pressure (Ψ_p^2) at ξ_1 or ξ_2	Isolator I *	15	13	10	9
		Isolator II **	17	17	6	7
Isolator location given moment excitation	Velocity (Ψ_v^2) at ξ_3 or ξ_4	Rubber I ***	22	22	20	18
		Aluminum I ***	7	4	11	6
		Polypropylene II ***	25	26	24	24
		Aluminum II ***	9	5	11	12
	Sound pressure (Ψ_p^2) at ξ_1 or ξ_2	Rubber I ***	21	22	15	15
		Aluminum I ***	7	8	7	8
		Polypropylene II ***	24	25	20	20
		Aluminum II ***	7	9	10	11

Table 6. Spectral averages of insertion losses for the experimental system of Figure 13.

Baseline for insertion loss calculation:
* system with Rubber isolator I
** system with Polypropylene isolator II
*** system with a mount located at the center of the mass source

4.3 Effect of isolator location

Next, the effects of mount location are examined using the experimental system of Figure 13. Only the rotational free velocity of the source should exist for the moment excitation case when a mount is located at the center of the mass source. And, both translational and rotational free velocities occur when the isolator is placed at the edge of the rigid body source [12]. Similar to the previous cases, insertion losses (*IL*) are calculated by using 2(a-c). In this case, subscript '*A*' and '*B*' refer to the cases when the isolator is placed at the edge and at the center of the mass respectively. First, consider the rubber and polypropylene isolator (I) cases of Figures 18(a, c) and 19(a, c), where both computational and experimental results show that all vibration, sound and power measures are significantly reduced when an isolator is moved from the edge to the mass center.

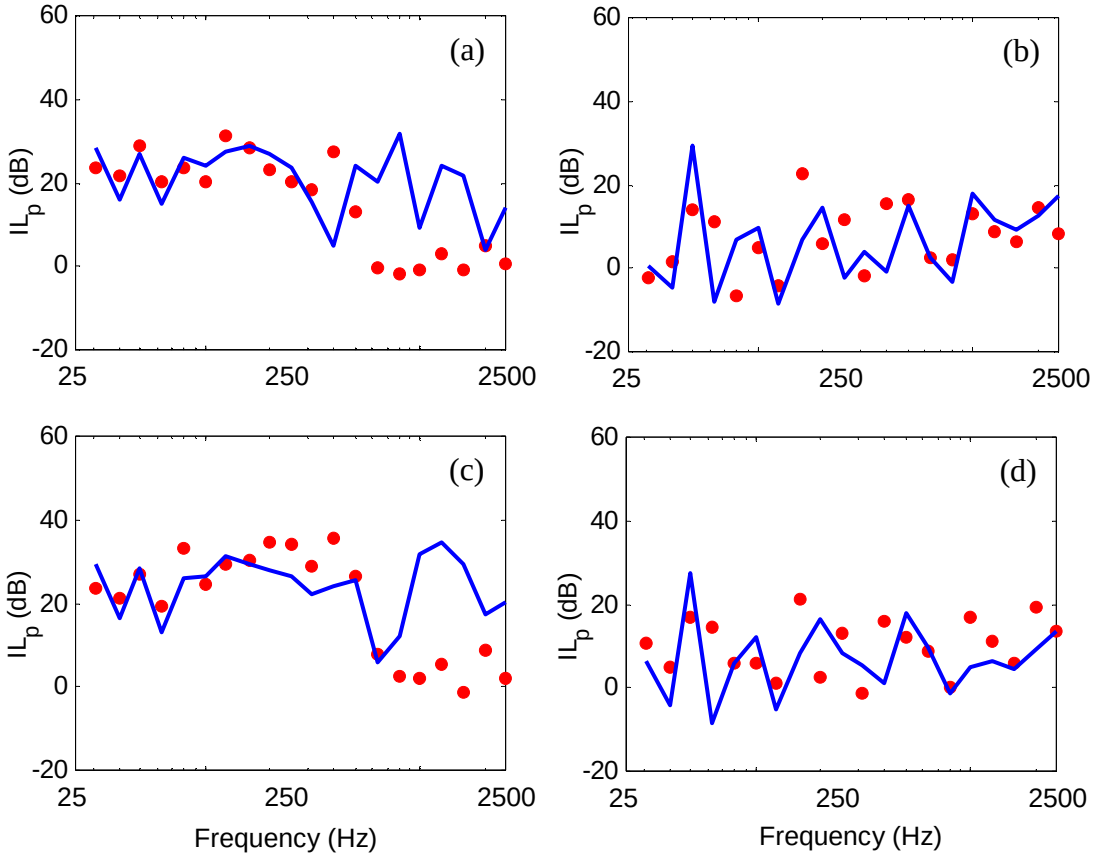

Figure 18. Insertion loss ($IL_{\Pi_{RAD}}$) of sound pressure at field location ξ_1 of Table 4 on mount location given moment excitation. (a) Rubber isolator I; (b) aluminum isolator I; (c) polypropylene isolator II; (d) aluminum isolator II. Key: ——— , calculated; ● , measured. Results are given in terms of 1/3 octave band center frequencies from 31.5 to 2500 Hz. Only the mean values within each bandwidth are plotted here.

Like the previous case, measured IL_p spectra do not exhibit as much reduction as the ones computed beyond 500 Hz because the actual sound radiated from the receiver is lower than the shaker noise beyond 500 Hz, especially when a rubber isolator is located at the center of source. Further, similar to the previous case, IL_v spectra beyond 500 Hz are much higher than IL_p since measured IL_v are not contaminated by the shaker noise.

Next, aluminum isolators (I and II) are examined. Figure 18(b, d) and 19(b, d) show that vibration and acoustic measures are reduced by connecting an aluminum mount at a source location with zero translational free velocity. However, the aluminum isolator cases show less reduction when compared to the rubber or polypropylene isolator case. Further, it is observed in Figures 18(b, d) that measured IL_p values exhibit a reasonable match with computed IL_p since the sound pressures with an aluminum mount are higher than the shaker noise level.

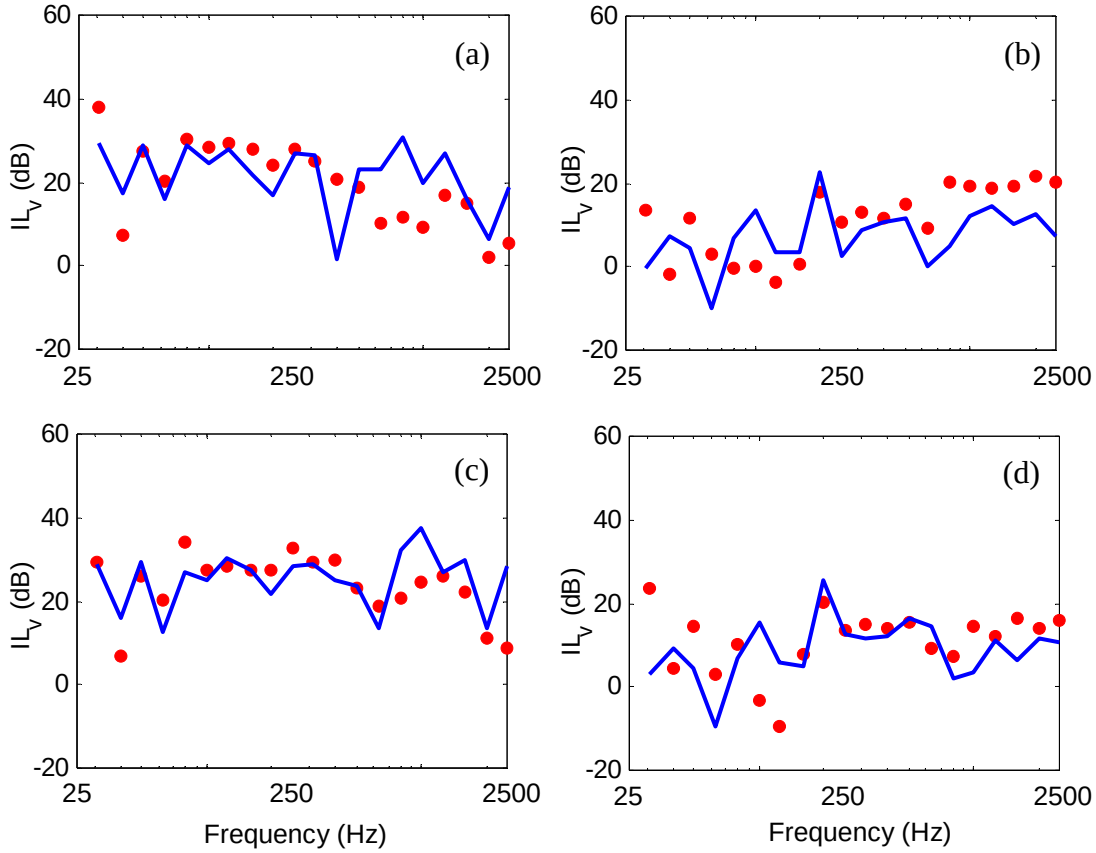

Figure 19. Insertion loss (IL_v) of velocity at plate location ξ_3 of Table 4 on mount location given moment excitation. (a) Rubber isolator I; (b) aluminum isolator I; (c) polypropylene isolator II; (d) aluminum isolator II. Key: ——— , calculated; ● , measured. Results are given in terms of 1/3 octave band center frequencies from 31.5 to 2500 Hz. Only the mean values within each bandwidth are plotted here.

Overall, IL_p spectra match well with Π_{RAD}, like the previous case. Similar to the mount material case, spectral averages of the measured and computed insertion losses are again shown in Table 6. It is observed that significant reductions in vibration transmission, based on mount locations, are identified by using sound pressure measures for a system with Rubber I or Polypropylene II isolator. Velocity measures at selected locations also provide large reductions in vibration transmitted to a receiver, as seen from Table 6. Further, some reductions in velocity and sound measures are observed for a system with an aluminum isolator. Like the previous case, reasonable agreements between computed and experimental results are observed even though some measurements are contaminated by the shaker noise as discussed before.

Conclusions

6.1 Summary

Several measures of vibration isolation performance have been critically examined for a multi-dimensional system with inverted 'L' structure receivers. Non-dimensional components of multi-dimensional transmissibilities and effectivenesses are comparatively evaluated for an inverted 'L' beam receiver and four source configurations. Radiated sound pressures resulting from both in-plane and out-of plane motions of the 'L' beam receiver, have also been calculated and correlated with power-based measures. Further, vibration power components transmitted to the 'L' beam receiver and their interactions have been analyzed. Our analysis shows that significant couplings occur between different degrees-of-freedom. In order to efficiently interpret transfer paths of inherent complexity, several measures have been examined. Sound measurements and predictions for the inverted 'L' plate demonstrate that a rank order based on free field sound pressures, at a properly selected point, could be regarded as a measure of the vibration power transmitted to the receiver. Measured insertion losses for sound pressure match well with those based on computed results, especially on the basis of spectrally-averaged values.

6.2. Emerging research issues

Properties of elastomeric and hydraulic isolators typically show frequency-dependency and are sensitive to preload and dynamic excitation levels [2, 3]. In order to properly predict the isolation behavior of such nonlinear systems, one must question the use of measures that are typically derived based on the linear system theory [34]. Several experimental methods have been developed to characterize the stiffnesses of an isolator. Direct force measures have been pursued by simulating ideal boundary conditions [35, 36] but such approaches are limited to lower frequencies since the unwanted dynamics of measurement machine is involved as the frequency increases [35]. Recently, some approximate methods that are based on motion transmissibilities have also been developed [37-40]. However, alternate laboratory measurement methods need to be correlated using appropriate isolation measures.

Simplified isolator models are often employed to describe a dynamic behavior of vibration isolation system [3, 5, 11, 15, 16, 41]. These are often longitudinal spring models [3, 5, 11] though some models include flexural components with or without the cross-axis coupling terms [15, 16, 41]. However, it is known that the rotational component becomes important and standing wave effects occur within an isolator as the frequency increases [1, 4, 41]. Therefore, more

advanced isolator models are needed to properly describe couplings among multiple and/or multi-dimensional transmission paths [12, 24-27]. Both driving and transfer point stiffnesses must be known to properly interpret isolator measures.

Several efforts have been made to quantify the contribution of source to vibration transmission to a receiver [12, 23-27]. One may introduce a source descriptor along with an effective mobility concept to quantify the source contribution [23-27]. Further, the role of free source velocity on vibration transmission has been emphasized [12] and recently a "pseudo-force" method has been developed to simulate the free velocities of a source [42-43]. However, a more appropriate quantification of source strength is still required and dynamic interactions between sources and paths would need further investigation, especially in the presence of compliant vibration sources. Finally, future work is required to properly interpret coupling phenomena and to develop efficient transfer path measures for 'real life' systems that incorporate multiple isolators. Efforts are also needed to identify appropriate measures for structure-borne and airborne noise paths over a broad range of frequencies.

Acknowledgements

The General Motors Corporation (Noise and Vibration Center) and the Goodyear Tire and Rubber Company (Transportation Molded Products) are gratefully acknowledged for supporting this research.

References

1. L. L. BERANEK 1988 *Noise and Vibration Control*. Washington, DC: Institute of Noise Control Engineering.
2. C. M. HARRIS 1987 *Shock and Vibration handbook*. New York: McGraw-Hill Book Company.
3. J. C. SNOWDON 1968 *Vibration and Shock in Damped Mechanical Systems*. New York: John Wiley & Sons, Inc.
4. E. E. UNGAR and C. W. DIETRICH 1966 *Journal of Sound and Vibration*, **4**(2), 224-241. High-Frequency Vibration Isolation.
5. J. I. SOLIMAN and M. G. HALLAM 1968 *Journal of Sound and Vibration*, **8**(2), 329-351. Vibration Isolation between Non-Rigid Machines and Non-Rigid Foundations.
6. N. M. M. MAIA, J. M. M. SILVA and A. M. R. RIBEIRO 2001 *Mechanical Systems and Signal Processing*, **15**(1), 129-137. The Transmissibility Concept in Multi-Degree-of-Freedom Systems.
7. D. A. SWANSON, L. R. MIILER and M. A. NORRIS 1994 *Journal of Aircraft*, **31**(1), 188-196. Multidimensional Mount Effectiveness for Vibration Isolation.
8. A. O. SYKES 1968 *Ph.D. Thesis, The Catholic University of America, Washington D. C., USA*. Development and Application of Linear Multi-Terminal Network Theory to Vibration Problems.
9. Y. K. KOH and R. G. WHITE 1996 *Journal of Sound and Vibration*, **196**(4), 495-508. Analysis and Control of Vibrational Power Transmission to Machinery Supporting Structures Subjected to a Multi-Excitation System, Part II: Vibrational Power Analysis and Control Schemes.

10. H. G. D. GOYDER and R. G. WHITE 1980 *Journal of Sound and Vibration*, **68**(1), 77-96. Vibrational Power Flow from Machines into Built-Up Structures, Part II: Wave Propagation and Power Flow in Beam-Stiffened Plates.
11. H. G. D. GOYDER and R. G. WHITE 1980 *Journal of Sound and Vibration*, **68**(1), 97-117. Vibrational Power Flow from Machines into Built-Up Structures, Part III: Power Flow Through Isolation Systems.
12. S. KIM and R. SINGH 2001 *Submitted to Journal of Sound and Vibration*, Source Characteristics of a Multi-Dimensional Vibration Isolation System.
13. R. J. PINNINGTON 1987 *Journal of Sound and Vibration*, **118**(3), 515-530. Vibrational Power Transmission to a Seating of a Vibration Isolated Motor.
14. R. J. PINNINGTON and R. G. WHITE 1981 *Journal of Sound and Vibration*, **75**(2), 179-197. Power Flow Through Machine Isolators to Resonant and Non-Resonant Beams.
15. J. PAN, J. PAN and C. H. HANSEN 1992 *Journal of the Acoustical Society of America*, **92**(2), 895-907. Total Power Flow from a Vibrating Rigid Body to a Thin Panel Through Multiple Elastic Mounts.
16. W. L. LI and P. LAVRICH 1999 *Journal of Sound and Vibration*, **224**(4), 757-774. Prediction of Power Flows Through Machine Vibration Isolators.
17. L. CREMER and M. HECKLE 1973 Structure-Borne Sound: Structural Vibrations and Sound Radiation at Audio Frequencies. New York: Springer-Verlag.
18. R. H. LYON and R. G. DEJONG 1995 Theory and Application of Statistical Energy Analysis. Boston: Butterworth-Heinemann.
19. T. E. ROOK and R. SINGH 1996 *Noise Control Engineering Journal* 44(2), 69-78. Mobility Analysis of Structure-borne Noise Power Flow through Bearings in Gearbox-like Structures.
20. P. GARDONIO, S. J. ELLIOTT and R. J. PINNINGTON 1997 *Journal of Sound and Vibration*, **207**(1), 61-93. Active Isolation of Structural Vibration on a Multiple-Degree-of-Freedom System, Part I: The Dynamics of the System.
21. S. KIM and R. SINGH 2001 *Journal of Sound and Vibration*, Vibration Transmission Through an Isolator Modeled by Continuous System Theory (in press).
22. R. H. LYON 1983 *Noise Control Engineering Journal*, May-June, 92-103. Vibration Transmission in Machine Structures.
23. J. M. MONDOT and B. A. T. PETERSSON 1987 *Journal of Sound and Vibration*, **114**(3), 507-518. Characterization of Structure-Borne Sound Sources: The Source Descriptor and the Coupling Function.
24. R. A. FULFORD and B. M. GIBBS 1997 *Journal of Sound and Vibration*, **204**(4), 659-677. Structure-Borne Sound Power and Source Characterisation in Multi-Point-Connected Systems, Part 1: Case Studies for Assumed Force Distributions.
25. R. A. FULFORD and B. M. GIBBS 1999 *Journal of Sound and Vibration*, **220**(2), 203-224. Structure-Borne Sound Power and Source Characterization in Multi-Point-Connected Systems, Part 2: About Mobility Functions and Free Velocities.
26. B. A. T. PETERSSON 1993 *Journal of Sound and Vibration*, **160**(1), 43-66. Use of Source Descriptor Concept in Studies of Multi-Point and Multi-Directional Vibrational Sources.
27. B. A. T. PETERSSON and J. PLUNT 1982 *Journal of Sound and Vibration*, **82**(4), 517-529. On Effective Mobilities in the Prediction of Structure-Borne Sound Transmission Between a Source and a Receiving Structure, Part 1: Theoretical Background and Basic Experimental Studies.

28. T. ten WOLDE and G. R. GADEFELT 1987 *Noise Control Engineering Journal*, January-February, 5-14. Development of Standard Measurement Methods for Structure-Borne Sound Emission.
29. S. KIM and R. SINGH 2000 *Journal of Sound and Vibration*, **245**(5), 877-913. Multi-Dimensional Characterization of Vibration Isolators over a Wide Range of Frequencies.
30. S. KIM and R. SINGH 2001 *Submitted to Journal of Sound and Vibration*. Examination of Multi-Dimensional Vibration Isolation Measures.
31. I-DEAS *Users manual version 8.2.* 2000 SDRC, USA.
32. SYSNOISE Users manual version 5.4. 1999 NIT, Belgium.
33. F. FAHY 1985 *Sound and Structural Vibration: Radiation, Transmission and Response.* London: Academic Press.
34. T. JEONG and R. SINGH 2001 *Journal of Sound and Vibration*, **245**(3), 385-415. Inclusion of Measured Frequency- and Amplitude-Dependent Mount Properties in Vehicle or Machinery Models.
35. MTS Systems Corporation 1999 Test Star II Control System User Manual - Dynamic characterization, Page 40.
36. S. NADEAU and Y. CHAMPOUX 2000 *Experimental Techniques*, May/June, 21-23. Application of the Direct Complex Stiffness Method to Engine Mounts.
37. D. J. THOMPSON and N. VINCENT 1995 *Vehicle System Dynamics Supplement*, **24**, 86-99. Track dynamic behavior of at High Frequencies. Part 1: Theoretical Models and Laboratory Measurements.
38. D. J. THOMPSON and J. W. VERHEIJ 1997 *Applied Acoustics*, **52**, 1-17. The Dynamic Behavior of Rail Fasteners at High Frequencies.
39. D. J. THOMPSON, W. J. VAN VLIET and J. W. VERHEIJ 1998 *Journal of Sound and Vibration*, **213**(1), 169-188. Development of the Indirect Method for Measuring the High Frequency Dynamic Stiffness of Resilient Isolator.
40. Å. FENANDER 1997 *Journal of Rail and Rapid Transit, Proceedings of I.Mech.E. Part F*, **211**, 51-62. Frequency Dependent Stiffness and Damping of Railpads.
41. M. A. SANDERSON 1996 *Journal of Sound and Vibration*, **198**(2), 171-191. Vibration Isolation: Moments and Rotations Included.
42. M. H. A. JANSSENS and J. W. VERHEIJ 1999 *Journal of Sound and Vibration*, **226**(2), 305-328. The Use of an Equivalent Forces Method for the Experimental Quantification of Structural Sound Transmission in Ships.
43. M. H. A. JANSSENS and J. W. VERHEIJ 2000 *Applied Acoustics*, **61**, 285-308. A Pseudo-forces Methodology to be Used in Characterization of Structure-borne Sound Sources.

Appendix A

b	width
d	distance to field point from reference
E	Young's modulus
f	force amplitude
F	excitation
$\mathbf{F}$	excitation vector

G	shear modulus
h	reference location in rigid body with respect to mass center
IL	insertion loss
j	$\sqrt{-1}$
ℓ	length
m	mass
M	mobility
$\mathbf{M}$	mobility matrix
p	sound pressure
q	moment amplitude
Q	numerical constant for rubber material
r	radius
S	area
S, P, R	source, path and receiver
t	thickness
T	shape factor
TR	transmissibility
$\mathbf{TR}$	transmissibility matrix
v	translational velocity
V	velocity
$\mathbf{V}$	velocity vector
x, y, z	cartesian coordinates
α, β, γ	mobilities of components
$\boldsymbol{\alpha}, \boldsymbol{\beta}, \boldsymbol{\gamma}$	mobility matrices of components
Γ	structural power efficiency
η	loss factor
θ	rotational displacement
ξ	response location
Ξ	effectiveness
$\boldsymbol{\Xi}$	effectiveness matrix
Π	vibration power (time-averaged)
ρ	mass density
Ψ	mean-square
ω	frequency, rad/sec

Subscripts

a	air
G	mass center
H	horizontal beam or plate
IN	input
i, j	indices or reference points
Q	variable
RAD	radiated

S, P, R	source, path and receiver
TR	transmitted out
V	vertical beam or plate
WF	weighted force
WV	weighted velocity
with	with isolator
without	without isolator
x, *y*, *z*	cartesian coordinates

Superscripts

b	blocked
f	free
T	transpose
~	complex valued
*	complex conjugate

Operators

diag	diagonal matrix
Re	real part
< >	time-averaged
/	quotient for matrices